EPJ Web of Conferences **346**, 02024 (2026) https://doi.org/10.1051/epjconf/202634602024
RFPPC2025

Initial electron cyclotron heating/current drive scoping study for the SMall Aspect Ratio Tokamak (SMART)

Nicola Bertelli[1,*], *Syun'ichi* Shiraiwa[1], *John W.* Berkery[1], *Masayuki* Ono[1], *Álvaro* Sánchez-Villar[1], *Diego J.* Cruz-Zabala[2], *Manuel* Garcia-Muñoz[2], *Carlos* López-Jiménez[2], *Jesús* Salas Suárez-Bárcena[2], and *Eleonora* Viezzer[2]

[1]Princeton Plasma Physics Laboratory, Princeton, 08540, NJ, USA
[2]Department of Atomic, Molecular and Nuclear Physics, University of Seville, Seville, Spain

Abstract. In this work an initial electron cyclotron heating/current drive (EC H&CD) scoping study is presented for the SMall Aspect Ratio Tokamak (SMART), constructed and operated by the Plasma Science and Fusion Technology (PSFT) Laboratory of the University of Seville. We consider two planned phases of operation with different magnitude of magnetic field ($B \simeq 0.4$, and 1 T). This EC H&CD scoping study is carried out by using the ray tracing code TRAVIS, which allows to quickly perform a series of scans on the main SMART plasma scenarios. A scan in the poloidal and toroidal launching angles is performed for the $B \simeq 0.4$ T plasma scenario assuming three launching locations (mid-plane, off-mid-plane, and top-launcher) and the extraordinary (X-) mode polarization. The absorption occurs at the second harmonic and, overall, the highest power absorption is obtained launching the EC beam from the top of the machine. A numerical analysis of the fundamental X-mode EC H&CD start-up regime for the $B \simeq 1.0$ T plasma scenario with two different wave frequencies (28 and 35 GHz) is presented showing a very high current drive efficiency.

1 Introduction

The SMall Aspect Ratio Tokamak (SMART), constructed and operated by the Plasma Science and Fusion Technology (PSFT) Laboratory of the University of Seville, had its first plasma in the end of 2024. SMART is a spherical tokamak (ST) with unique flexible shaping capabilities, which will allow it to operate at both negative and positive triangularity [1]. Installation and commissioning of a neutral beam injection (NBI) system for auxiliary heating is also ongoing [2]. Therefore, this device is an ideal platform for testing RF heating/current drive (H&CD) schemes in a wide range of ST operational regimes. Moreover, RF actuators would also significantly expand the SMART operation regimes.

For this reason, in this work we survey electron cyclotron (EC) heating and current drive (H&CD) scheme for anticipated SMART plasma scenarios. We consider two of the three planned phases of operations [2, 3] with different magnitude of magnetic field ($B \simeq 0.4$ and 1 T). Initial SMART operational phase with lower B field is expected to make the EC H&CD scheme more attractive whereas for higher field operation different and/or a combination of H&CD schemes can, in principle, be considered. This EC H&CD scoping study is carried out by using the ray tracing model TRAVIS code [4], which allows to quickly perform a series of scans on the main SMART plasma scenarios. The structure of the paper is as follows: electron cyclotron (EC) power deposition for $B = 0.4$ T at the second cyclotron resonance is described in Section 2. In Section 3 the EC power deposition and current drive for $B = 1.0$ T plasma scenario at the first harmonic are presented performing different parameters scans. Conclusions are provided in Section 4.

2 Electron cyclotron power deposition for B = 0.4 T plasma scenario

In this Section we analyze the electron cyclotron (EC) power absorption for the $B = 0.4$ T SMART plasma scenario (as shown in Figure 1) by making use of the ray tracing code TRAVIS [4]. Assuming a wave frequency of 28 GHz, we have three electron cyclotron resonances in the vacuum vessel domain ($n = 1, 2$ and 3), where two of them are within the last closed flux surface ($n = 2$ and 3). Three launching positions are considered: mid-plane launcher at ($R = 0.8$ m, $Z = 0$ m), off-mid-plane launcher at ($R = 0.8$ m, $Z = 0.4$ m), and top launcher at ($R = 0.5$ m, $Z = 0.8$ m). These constitute realistic future locations for SMART, as they correspond to the locations of vacuum vessel parts [5]. All the kinetic profiles are considered parabolic profiles and a difference of one order of magnitude between the central and edge values is assumed. For all the simulations, an eXtraordinary (X-) mode polarization is considered, which has a larger absorption with respect to the ordinary (O-) mode. In these simulations, in terms of launching angles, we use the angles employed in the ITER benchmark code activity and studies [18]: the poloidal steering angle α, defined as the angle between the horizontal plane (constant Z) and the poloidal component of the beam, and the toroidal steering angle β, defined

*Corresponding author: nbertell@pppl.gov

as the angle between the beam and the poloidal plane. α and β angles are therefore related to the "common" polar angle θ and the azimuthal angle ϕ. The relationships between the two pairs are as fellows: $\theta = \arccos(\cos\beta\sin\alpha)$ $\phi = \pi + \arcsin(\sin\beta/\sin\theta)$. In all the simulations shown below we assume one single ray. Finally, the main focus of this initial analysis is on the maximum EC power absorption achieved in some plasma conditions.

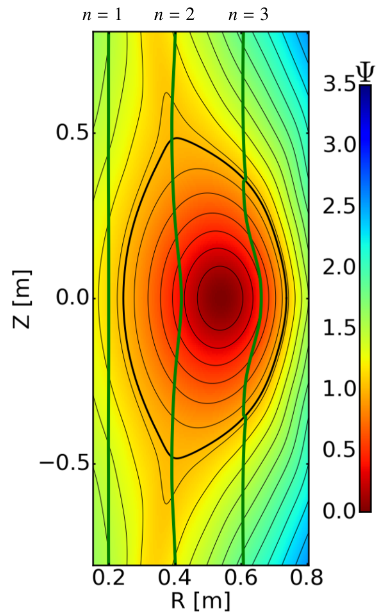

Figure 1. Magnetic equilibrium for $B = 0.4$ T used in the simulations. The thick dark green curves represent the $n = 1, 2$ and 3 electron cyclotron resonances. The thick black curve represents the last closed flux surface. Plasma current is 0.2 MA.

2.1 Mid-plane launcher

An example of a EC ray trajectory launched at the mid-plane for $f = 28$ GHz and X-mode is shown in Figure 2. In this case, the central density is $n_{e,0} = 2.0 \times 10^{18}$ m^{-3} and central temperature of $T_{e,0} = 0.5$ keV. Moreover, the launching angles are $\alpha = 10°$ and $\beta = 20°$. The ray crosses both the second and third harmonics but a negligible EC absorption occurs on the third harmonic. For this plasma scenario, the X-cut-off starts to appear in the second harmonic around the mid-plane for central density of $n_{e,0} = 5.6 \times 10^{18}$ m^{-3}.

For the mid-plane launcher we perform a scan in the toroidal angle β (0° to 30°) with $\alpha = 0°$ assuming two low density cases: $n_{e,0} = 1.0 \times 10^{18}$ m^{-3} and $n_{e,0} = 1.5 \times 10^{18}$ m^{-3} and two temperature values: $T_{e,0} = 0.5$ keV and $T_{e,0} = 1.0$ keV. The maximum EC absorption for these cases is summarized in the Table 1 indicating also the range in the toroidal launching angle β. As expected, EC absorption is increasing with increasing temperature and density. Up to 40% of power can be absorbed in the case of $n_{e,0} = 1.5 \times 10^{18}$ m^{-3} and $T_{e,0} = 1.0$ keV. Another case at higher density, $n_{e,0} = 5.5 \times 10^{18}$ m^{-3}, just below the appearance of X-cut-off density, is also shown in Table 1. For $T_{e,0} = 1.0$ keV, 68% of EC power absorption is achieved for a narrow range of the toroidal angle β (3° − 5°). In general, as shown in both Tables 1, we found a quite narrow range of the toroidal angle β where EC absorption is peaked. For lower density a larger toroidal angle β ($17° \lesssim \beta \lesssim 22°$) is required to achieved the maximum EC absorption with respect to the high density case. In these simulations we have only assumed the poloidal angle $\alpha = 0°$ in order to point the EC ray towards the center of the plasma where both density and temperature have their maximum values. However, one could consider higher density cases ($n_{e,0} > 5.5 \times 10^{18}$ m^{-3}) with the presence of the X-cut-off layer, launching the EC beam with $\alpha \neq 0°$. This will be part of a separate work.

2.2 Off-mid-plane

As shown in subsection 2.1, a similar set of simulations is also presented for the off-mid-plane case which corresponds to a launching position of ($R = 0.8$ m, $Z = 0.4$ m). The plasma parameters are the same used in the previous subsection except for the poloidal launching angle α, which is assumed to be −45° in order to point the EC beam towards the center of the plasma. For the off-mid-plane launcher, at lower density cases, we found slightly higher EC power absorption with respect to the mid-plane launcher for both the temperature values with a similar β angle (19° − 20°) as shown in Table 2. For $n_{e,0} = 5.5 \times 10^{18}$ m^{-3}, a similar EC absorption is obtained with respect to the mid-plane case, but with a wider β angle range.

2.3 Top launcher

A third EC launching angle scan is performed assuming a top launcher ($R = 0.5$ m, $Z = 0.8$ m). The SMART machine has poloidal field coils inside of the vacuum vessel, but in this work we do not assess if there is any physical room for a potential EC top launcher. In any case, we perform this set of simulations to understand the trend of the EC power absorption with respect to the previous two launching positions.

For this top launcher case, in order to point the EC beam toward the center of the plasma we scanned α angle between 75° and 85° considering five different β angle values (5°, 10°, 15°, and 20°) as indicated in Tables 4, 5, and 6. Density and temperature values are the same as the ones used in the previous subsections. In this case we found a significantly higher EC power absorption with respect to the previous cases. For $T_{e,0} = 1.0$ keV, EC power absorption is larger than 80%, except for a couple of cases for $n_{e,0} = 1.0 \times 10^{18}$ m^{-3} at ∼ 70% absorption level. Having an EC beam more parallel to the EC resonance allow for better performance in terms of EC power absorption and current drive (not shown here). This is consistent with previous studies [6–12] and DIII-D experimental results [13].

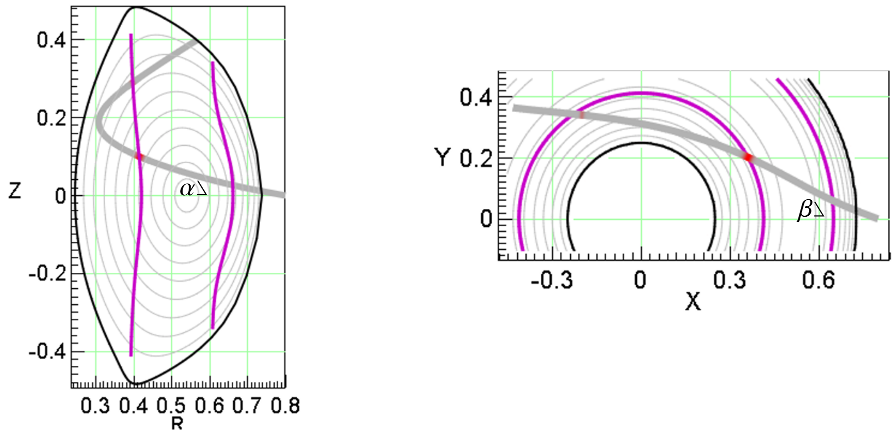

Figure 2. Poloidal (left) and toroidal (right) projection of the EC ray trajectory launched at the mid-plane for f = 28 GHz, B = 0.4 T, central density of $n_{e,0} = 2.0 \times 10^{18}$ m^{-3} and central temperature of $T_{e,0}$ = 0.5 keV with X-mode polarization evaluated by the TRAVIS code. The launching angles are: α = 10° and β = 20° (their are indicated in the figures for reference). Magenta curves indicate the second and third EC cyclotron resonances. The red spot indicates the region where EC absorption occurs.

Table 1. EC absorption (in percentage) for B = 0.4 T plasma scenario and mid-plane launcher with α = 0° and β = [0° – 30°].

$\alpha = 0°$	$n_e = 1.0 \times 10^{18}$ m^{-3}	$n_e = 1.5 \times 10^{18}$ m^{-3}	$n_e = 5.5 \times 10^{18}$ m^{-3}
$T_{e,0}$ = 0.5 keV	**17%** (β = 19° – 21°)	**23%** (β = 17° – 21°)	**45%** (β = 3° – 5°)
$T_{e,0}$ = 1.0 keV	**30%** (β = 17° – 22°)	**40%** (β = 17° – 22°)	**68%** (β = 3° – 5°)

Table 2. EC absorption (in percentage) as in Table 1 for off- mid-plane launcher condition with α = −45° and β = [0° – 30°].

$\alpha = -45°$	$n_e = 1.0 \times 10^{18}$ m^{-3}	$n_e = 1.5 \times 10^{18}$ m^{-3}
$T_{e,0}$ = 0.5 keV	**17% - 23%** (β = 20° – 21°)	**33%** (β = 20°)
$T_{e,0}$ = 1.0 keV	**25% - 35%** (β = 19° – 21°)	**38% - 51%** (β = 19° – 20°)

Table 3. EC absorption (in percentage) as in Table 2 with higher density.

$\alpha = -45°$	$n_e = 5.5 \times 10^{18}$ m^{-3}
$T_{e,0}$ = 0.5 keV	**36% - 43%** (β = 2° – 13°)
$T_{e,0}$ = 1.0 keV	**58% - 65%** (β = 0° – 12°)

Table 4. EC absorption (in percentage) as in Table 1 for top launcher condition with 75° ≤ α ≤ 85° and β = [0°, 5°, 10°, 15°, 20°].

	$n_e = 1.0 \times 10^{18}$ m^{-3}				
β	0°	5°	10°	15°	20°
$T_{e,0}$ = 0.5 keV	**68%**	**45%**	**75%**	**65%**	**53%**
$T_{e,0}$ = 1.0 keV	**85%**	**70%**	**87%**	**81%**	**73%**

Table 5. EC absorption (in percentage) as in Table 4 for density of 1.5×10^{18} m^{-3}.

	$n_e = 1.5 \times 10^{18}$ m^{-3}				
β	0°	5°	10°	15°	20°
$T_{e,0}$ = 0.5 keV	**68%**	**62%**	**71%**	**69%**	**69%**
$T_{e,0}$ = 1.0 keV	**87%**	**84%**	**89%**	**94%**	**85%**

Table 6. EC absorption (in percentage) as in Table 4 for density of 5.5×10^{18} m^{-3}.

	$n_e = 5.5 \times 10^{18}$ m^{-3}				
β	0°	5°	10°	15°	20°
$T_{e,0}$ = 0.5 keV	**61%**	**57%**	**50%**	**44%**	**44%**
$T_{e,0}$ = 1.0 keV	**84%**	**80%**	**74%**	**68%**	**67%**

3 X-I mode for B = 1 T plasma scenario

In this Section we analyze the electron cyclotron (EC) power absorption and the total EC current drive for the B = 1.0 T SMART plasma scenario (as shown in Figure 3). Assuming a wave frequency of 28 GHz, as in the previous section, the first (n = 1) EC resonance is exactly in the plasma core as indicated by the thick green curve in Figure 3. Quite recently, a new EC scheme for start-up plasma has been proposed [14–16]: launching a X-mode from the low field side when the plasma conditions are such that the EC resonance and the X-cut-off layers are very close. In this situation, due to the Doppler effect (broadening of the EC resonance) and the X-mode polarization, a large EC absorption can occur, driving a significant EC current. We want to explore here this EC scheme for the SMART device with B = 1 T plasma. It is important to mention that in this work we are evaluating the EC power deposition and EC current drive in the linear regime without considering potential nonlinear effects due to the low density scenario [17].

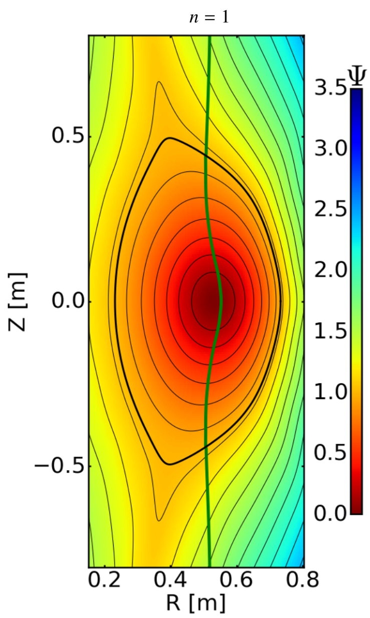

Figure 3. Magnetic equilibrium for B = 1.0 T used in the simulations. The thick dark green (black) curve represents the first electron cyclotron resonance (the last closed flux surface). Plasma current is 0.5 MA.

Figure 4 shows the poloidal and toroidal projections of the EC ray trajectory launched at the mid-plane with a central density of $n_{e,0} = 2.0 \times 10^{17}$ m^{-3}, central temperature of $T_{e,0}$ = 0.2 keV, and X-mode polarization. The launching angles are $\alpha = 0°$ and $\beta = 25°$. In this figure, magenta and red curves represent the fundamental EC resonance and the X-cut-off. For low density cases, the EC resonance and the X-cut-off are extremely close and, as a consequence, with a toroidal steering angle β different than zero, EC power absorption can occur. A toroidal angle β scan is shown in Figure 5 in terms of EC power deposition (left figures) and EC total driven current (right figures) assuming two wave frequencies, f = 28 (top figures) GHz and f = 35 GHz (bottom figures) and two temperature values: $T_{e,0}$ = 0.1 keV (blue curves) and $T_{e,0}$ = 0.1 keV (red curves). One can see that for a wide β angle range ($15° \lesssim \beta \lesssim 35°$), the EC power absorption is basically 100% for the case of $T_{e,0}$ = 0.2 keV (red curve) and for both wave frequency values. For f = 35 GHz, even the case with $T_{e,0}$ = 0.1 keV has an EC power absorption above 95%.

In terms of total EC driven current, we obtain a very significant current (right figures): for the case of f = 28 GHz, up to 1 MA/MW (up to 2.5 MA/MW) with $T_{e,0}$ = 0.1 keV ($T_{e,0}$ = 0.2 keV); for the case of f = 35 GHz, up to 1 MA/MW (up to 3.0 MA/MW) with $T_{e,0}$ = 0.1 keV ($T_{e,0}$ = 0.2 keV). As a reference, the reader can compare the EC driven current per MW evaluated for the ITER case (ECCD for neoclassical tearing modes suppression) by different EC codes in Table 2 of Ref. [18]. The operational phase 3 of SMART is planning a plasma current of 550 kA [2]. Therefore, these numerical results suggest 200-500 kW EC input power should be enough to obtain such a current for the plasma parameters used in the simulations.

From these simulations, it appears quite clear the strong dependency of the temperature on the EC driven current in agreement with the previous works [14]. As mentioned above, an assessment of the nonlinear effects on the EC driven current will be part of a separate work. A density scan ($1.0 \times 10^{16} \leq n_{e,0} \leq 1.0 \times 10^{18}$) is also shown in Figure 6 for both wave frequencies, $T_{e,0}$ = 0.2 keV, α = 0° and β = 25°. It appears that the EC power absorption rapidly decreases with increasing density ($n_{e,0} \gtrsim 2.5{\times}10^{17}$). This is due to the fact that for higher density the distance between the EC resonance and the X-cut-off layer increases as well. However, a quite large EC driven current (1-2 MA/MW) is found even for a reduced absorption case (40-80% absorption). Higher wave frequency can relax the constraint on the density as indicated

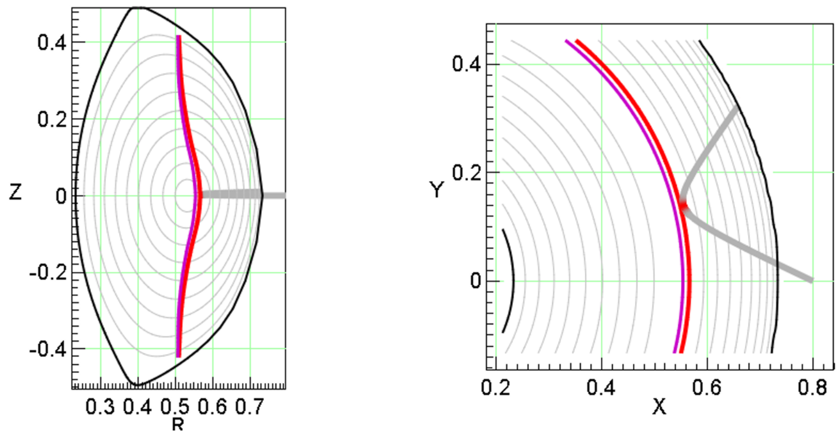

Figure 4. Poloidal (left) and toroidal (right) projection of the EC ray trajectory launched at the mid-plane for $f = 28$ GHz, $B = 1.0$ T, central density of 2.0×10^{17} m^{-3} and central temperature of 0.2 keV with X-mode polarization evaluated by the TRAVIS code. The launching angles are: $\alpha = 0°$ and $\beta = 25°$. Magenta and red curves indicate the first EC cyclotron resonance and X cut-off, respectively. The red spot indicates the region where EC absorption occurs.

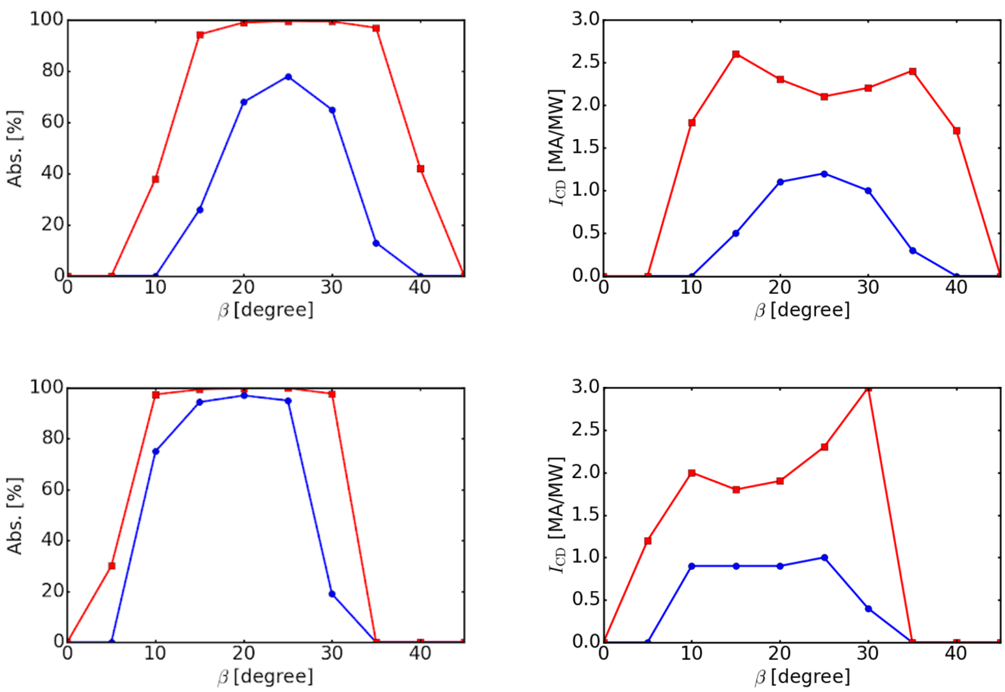

Figure 5. EC power absorption (left) and total EC current drive (right) per MW as a function of the β angle for $f = 28$ GHz (top) and $f = 35$ GHz (bottom), $\alpha = 0°$, and 1.0×10^{17} m^{-3}. $T_e = 0.1$ keV (0.2 keV) results are indicated in blue (red).

in Figure 6 by the red curve with respect to the blue curve. Figure 7 shows a scan of the central temperature, $T_{e,0}$ for both wave frequency cases (28 and 35 GHz) and with the same launching angles used in Figure 6. The top (bottom) row of Figure 7 shows the EC power absorption (left) and the total EC current drive (right) per MW for 28 GHz (35 GHz). Four (Five) different values of the central density are used for 28 GHz (35 GHz) as indicated in the figures. One can note that EC power absorption increased significantly with the electron temperature. Higher density cases with EC absorption well below 100% level still provide a very high current drive. Higher wave frequency allows higher EC power absorption at lower temperature and higher density with a very strong EC current drive efficiency.

4 Conclusions

In this work we have performed an initial EC H & CD study of the SMART device assuming two phases of operation with different magnitudes of magnetic field ($B \simeq 0.4$, and 1 T). This numerical analysis was performed by using the ray tracing code TRAVIS. For $B \simeq 0.4$ T plasma

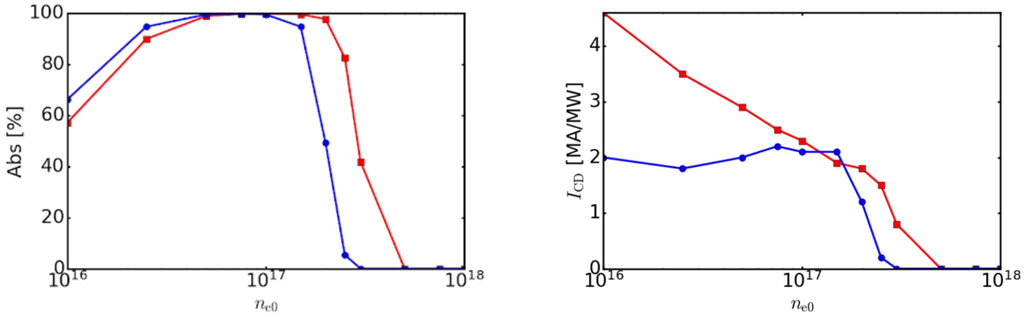

Figure 6. EC power absorption (left) and total EC current drive per MW (right) as a function of the central electron density ($n_{e,0}$ in m^{-3}) for f = 28 GHz (blue) and f = 35 GHz (red), $\alpha = 0°, \beta = 25°$, and T_e = 0.2 keV.

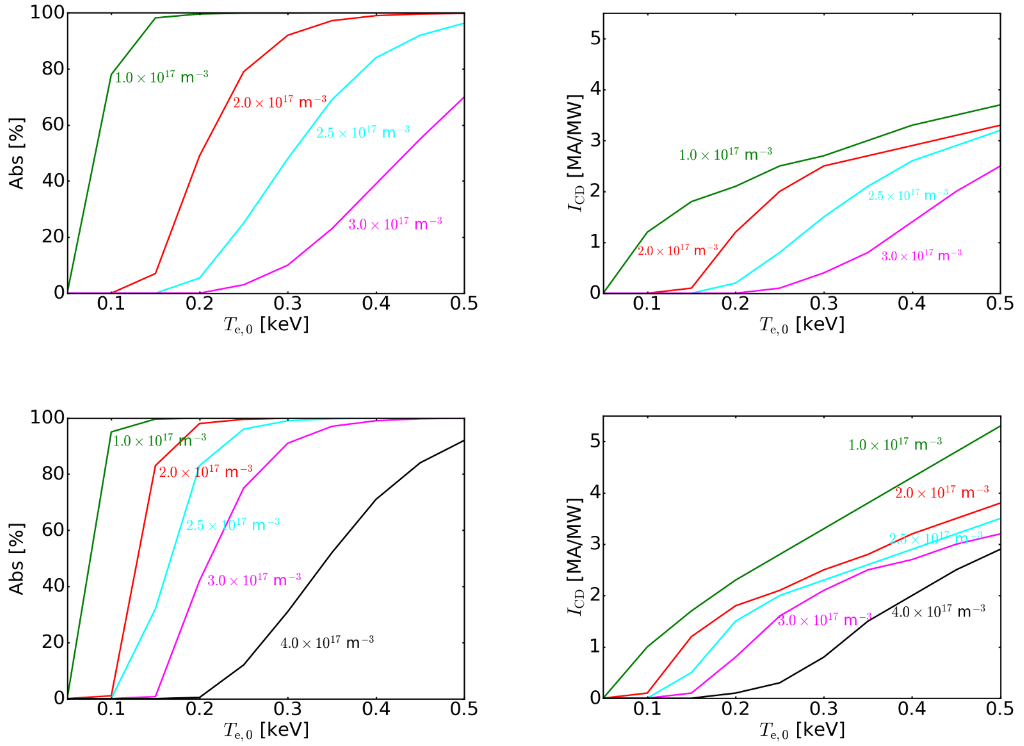

Figure 7. EC power absorption (left) and total EC current drive per MW (right) as a function of the central temperature $T_{e,0}$ for f = 28 GHz (top) and f = 35 GHz (bottom), $\alpha = 0°$, and $\beta = 25°$. The values of the central density $n_{e,0}$ are indicated in the figures.

scenario, the EC power is absorbed at the second harmonic assuming an X-mode polarization. Three different antenna locations were considered showing, as expected, that the the top launcher provides the highest EC power absorption. The fact that SMART has the poloidal field coils inside of the vessel makes the top launcher potentially not a feasible option. However, additional investigations are necessary to completely assess such possibility. For $B \simeq 1.0$ T plasma scenario, we have investigated the X-mode EC H&CD start-up regime as recently proposed [14–16]. Two wave frequencies (28 GHZ and 35 GHz) were considered. As in the previous works [14–16], we have found a very efficient EC driven current drive making this scheme very attractive for the start-up phase at low density particularly for spherical tokamaks. In this work, the EC power deposition and EC current drive have been evaluated in the linear regime without considering potential nonlinear effects due to the low density regime [17]. These nonlinear effects will be presented in a separate work. Moreover, it is important to note that, as in the previous works, we have assumed fully formed plasmas even though we have considered start-up plasma parameters.

5 Acknowledgment

This work was supported by the U.S. Department of Energy under contract number DE-AC02-09CH11466. The United States Government retains a non-exclusive, paid-up, irrevocable, world-wide license to publish or reproduce the published form of this manuscript, or allow others to do so, for United States Government purposes. One of the authors (N. B.) thanks Dr. N. B. Marushchenko for providing the TRAVIS source code.

References

[1] D. J. Cruz-Zabala et al., Performance prediction applying different reduced turbulence models to the SMART tokamak, Nucl. Fusion **64**, 126071 (2024). https://doi.org/10.1088/1741-4326/ad8a70

[2] A. Mancini et al., Predictive simulations for plasma scenarios in the SMART tokamak, Fus. Eng. Des. **192**, 11833 (2023). https://doi.org/10.1016/j.fusengdes.2023.113833

[3] M. Podestà et al., NBI optimization on SMART and implications for scenario development, Plasma Phys. Control. Fusion **66**, 045021 (2024). https://doi.org/10.1088/1361-6587/ad2edc

[4] N. B. Marushchenko, Y. Turkin, and H. Maassberg, Ray-tracing code TRAVIS for ECR heating, EC current drive and ECE diagnostic, Comput. Phys. Commun. **185**, 165 (2014). https://doi.org/10.1016/j.cpc.2013.09.002

[5] A. Mancini et al., Mechanical and electromagnetic design of the vacuum vessel of the SMART tokamak, Fus. Eng. Des. **171**, 112542 (2021). https://doi.org/10.1016/j.fusengdes.2021.112542

[6] K. Hamamatsu and A. Fukuyama, Numerical analysis of electron cyclotron current drive with suppressed Doppler broadening, Plasma Phys. Control. Fusion **42**, 1309 (2000). https://doi.org/10.1088/0741-3335/42/12/306

[7] R. W. Harvey and F. W. Perkins, Comparison of optimized ECCD for different launch locations in a next step tokamak reactor plasma, Nucl. Fusion **41**, 1847 (2001). https://doi.org/10.1088/0029-5515/41/12/312

[8] E. Poli et al., Electron-cyclotron-current-drive efficiency in DEMO plasmas, Nucl. Fusion **53**, 013011 (2013). https://doi.org/10.1088/0029-5515/53/1/013011

[9] A. M. Garofalo et al., Progress in the physics basis of a Fusion Nuclear Science Facility based on the Advanced Tokamak concept, Nucl. Fusion **54**, 073015 (2014). https://doi.org/10.1088/0029-5515/54/7/073015

[10] Y.-s. Bae, W. Namkung and M. H.Cho, Ray Tracing Study on Top ECCD Launch in KSTAR, EPJ Web Conf. **157** 03003 (2017). https://doi.org/10.1051/epjconf/201715703003

[11] E. Poli et al., Fast evaluation of the current driven by electron cyclotron waves for reactor studies, Phys. Plasmas **25**, 122501 (2018). https://doi.org/10.1063/1.5050345

[12] Xi. Chen et al., Top Launch for Higher Off-axis Electron Cyclotron Current Drive Efficiency, EPJ Web Conf. **203**, 01004 (2019). https://doi.org/10.1051/epjconf/201920301004

[13] Xi. Chen et al., Doubling off-axis electron cyclotron current drive efficiency via velocity space engineering, Nucl. Fusion **62**, 054001 (2022). https://doi.org/10.1088/1741-4326/ac544a

[14] M. Ono et al., Efficient electron cyclotron current drive regime for plasma current start-up in fusion reactors, Phys. Review E **106**, L023201 (2022). https://doi.org/10.1103/PhysRevE.106.L023201

[15] M. Ono et al., Time dependent model for non-inductive ECH X-I current ramp-up for SHPD tokamak facility, AIP Conference Proceedings **2984**, 110002 (2023). https://doi.org/10.1063/5.0163394

[16] M. Ono et al., Efficient ECCD non-inductive plasma current start- up, ramp-up, and sustainment for an ST fusion reactor, Nucl. Fusion **64**, 086021 (2024). https://doi.org/10.1088/1741-4326/ad556f

[17] R. W. Harvey, M. G. McCoy and G. D. Kerbel, Power Dependence of Electron-Cyclotron Current Drive for Low- and High-Field Absorption in Tokamaks, Phys. Rev. Lett. **62**, 426 (1989). https://doi.org/10.1103/PhysRevLett.62.426

[18] R. Prater et al., Benchmarking of codes for electron cyclotron heating and electron cyclotron current drive under ITER conditions, Nucl. Fusion **48**, 035006 (2008). https://doi.org/10.1088/0029-5515/48/3/035006